ACS APPLIED MATERIALS & INTERFACES

Research Article

www.acsami.org

Improved Electrochemical Performance of Fe-Substituted $NaNi_{0.5}Mn_{0.5}O_2$ Cathode Materials for Sodium-Ion Batteries

Ding D. Yuan, Yan X. Wang, Yu L. Cao,* Xin P. Ai, and Han X. Yang

College of Chemistry and Molecular Science, Wuhan University, Wuhan 430072, China

ABSTRACT: A series of O3-phase $NaFe_x(Ni_{0.5}Mn_{0.5})_{1-x}O_2$ (x = 0, 0.1, 0.2, 0.3, 0.4, and 1) samples with different Fe contents was prepared and investigated as high-capacity cathodic hosts of Na-ion batteries. The partial substitution of Ni and Mn with Fe in the O3-phase lattice can greatly improve the electrochemical performance and the structural stability. A $NaFe_{0.2}Mn_{0.4}Ni_{0.4}O_2$ cathode with an optimized Fe content of x = 0.2 can deliver an initial reversible capacity of 131 mAh g^{-1}, a reversible capacity greater than 95% over 30 cycles, and a high rate capacity of 86 mAh g^{-1} at 10 C in a voltage range of 2.0−4.0 V. The structural characterizations reveal that pristine $NaMn_{0.5}Ni_{0.5}O_2$ and Fe-substituted $NaFe_{0.2}Mn_{0.4}Ni_{0.4}O_2$ lattices underwent different phase transformations from P3 to P3″ and from P3 to OP2 phases, respectively, at high voltage interval. The as-resulted OP2 phase by Fe substitution has smaller interslab distance (5.13 Å) than the P3″ phase (5.72 Å), which suppresses the co-insertion of the solvent molecules, the electrolyte anions, or both and therefore enhances the cycling stability in the high voltage charge. This finding suggests a new strategy for creating cycle-stable transition-metal oxide cathodes for high-performance Na-ion batteries.

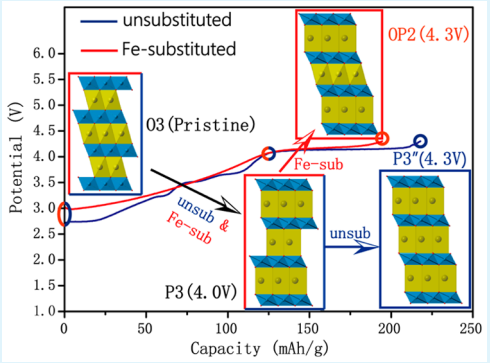

KEYWORDS: *$NaNi_{0.5}Mn_{0.5}O_2$, Fe substitution, transition metal oxides, sodium-ion batteries*

1. INTRODUCTION

Rechargeable batteries have recently garnered much attention for large-scale electric storage applications, such as for electric vehicles and renewable power stations. Due to the resource and cost limitations, lithium-ion batteries cannot support such large-scale applications. As a next-generation battery, sodium-ion batteries (SIBs) offer an attractive alternative to their lithium counterpart and have attracted increasing interest due to their low cost and abundant raw resources of sodium.[1−3] Among the sodium storage materials, a number of anode materials have exhibited considerably high reversible capacities and long-term cycling stability, for example, hard carbon (250−300 mAh g^{-1})[4,5] or Sb alloy (600 mAh g^{-1}).[6]

Meanwhile, various host materials such as transition metal oxides,[7−11] polyanion materials,[12−15] and Prussian blue frameworks[16−18] have been widely studied for sodium storage cathodes. Mainly, Na_xMO_2 type sodium transition-metal oxides (M = Co, Fe, Mn, V, Ni, etc.) have received attention as Na^+ host cathodes.[7−9] These sodium storage oxides have been classified into P2- and O3-type phases by Delmas,[19] where Na^+ occupies the prismatic (P) and octahedral (O) sites between the MO_2 layers in a unit cell. Various phases mainly depend on Na^+ defect or content in the transition metal oxides. In general, the P-type materials have a larger interlayer distance (e.g., 5.45 Å for $Na_{0.68}CoO_2$[20]) than that of O-type materials (e.g., 5.20 Å for $NaCoO_2$[20]), which leads to different sodium storage properties. O3-$NaNi_{1/2}Mn_{1/2}O_2$ delivers a discharge capacity of 125 mAh g^{-1} between 3.8 and 2 V, with 75% capacity retention after 50 cycles at 0.2 C, while P2−$Na_{2/3}Ni_{1/3}Mn_{2/3}O_2$ has a high capacity of 161 mAh g^{-1} with poor cycle stability;[21,22] O3-$NaFe_{1/2}Mn_{1/2}O_2$ delivered a capacity of 110 mAh g^{-1} in the potential range of 1.5−4.3 V, whereas P2−$Na_{2/3}Fe_{1/2}Mn_{1/2}O_2$ gave a high capacity of 190 mAh g^{-1}.[23] It is well-accepted that O3-type oxides have a lower reversible capacity but a good cycling stability, while P2-type oxides present a higher capacity but a limited cycle life. Besides, the need to release initial extra capacity due to high Na^+ defects in the P2-type oxides is also a severe obstacle for the practical battery applications. Therefore, great efforts have been devoted to improve the reversible capacity and cycling stability with decreasing content of the expensive elements (Co, Ni, etc.) for the O3-type oxides.

O3-$NaNi_{0.5}Mn_{0.5}O_2$ is one of most promising Na-storage cathodes due to its high capacity (>120 mAh g^{-1}) and cycling performance (81% capacity retention after 20th cycle), which were first reported by Komaba et al.[24] Subsequently, they substituted $Ni_{1/2}Mn_{1/2}$ with Fe in the O3-$NaFeO_2$ to form the O3-$NaFeO_2$−$NaNi_{1/2}Mn_{1/2}O_2$ solid solution (or O3-$NaFe_x(Ni_{1/2}Mn_{1/2})_{1-x}O_2$),[25] and suggested the O3-$NaFe_{0.4}(Ni_{1/2}Mn_{1/2})_{0.6}O_2$ as an optimum material by a trade-off of the capacity, cycling stability and cost. The O3-$NaFe_{1/3}Ni_{1/3}Mn_{1/3}O_2$ ($NaFe_{0.4}(Ni_{1/2}Mn_{1/2})_{0.6}O_2$) material with lower Fe amount was also reported to demonstrate good cyclability from 120 mAh g^{-1} in first cycle to ∼100 mAh

Received: January 20, 2015
Accepted: April 7, 2015
Published: April 7, 2015

DOI: 10.1021/acsami.5b00594
ACS Appl. Mater. Interfaces 2015, 7, 8585−8591

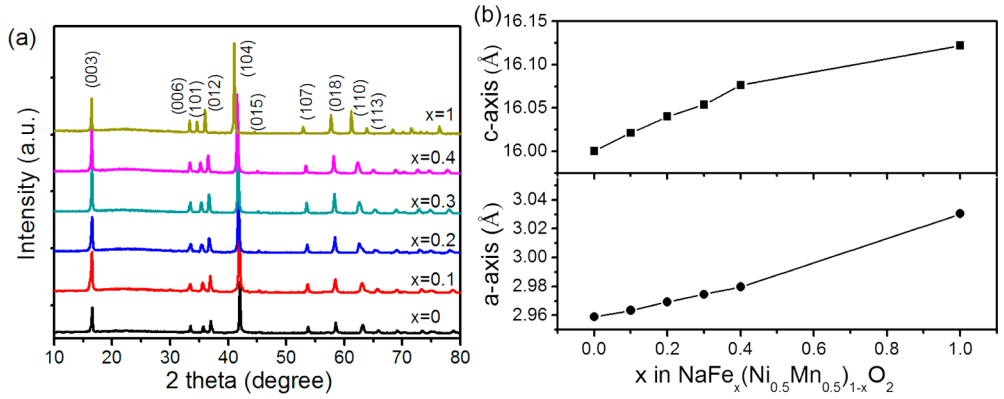

Figure 1. (a) XRD patterns and (b) lattice parameters of $NaFe_x(Ni_{0.5}Mn_{0.5})_{1-x}O_2$ (x = 0, 0.1, 0.2, 0.3, 0.4, 1) samples.

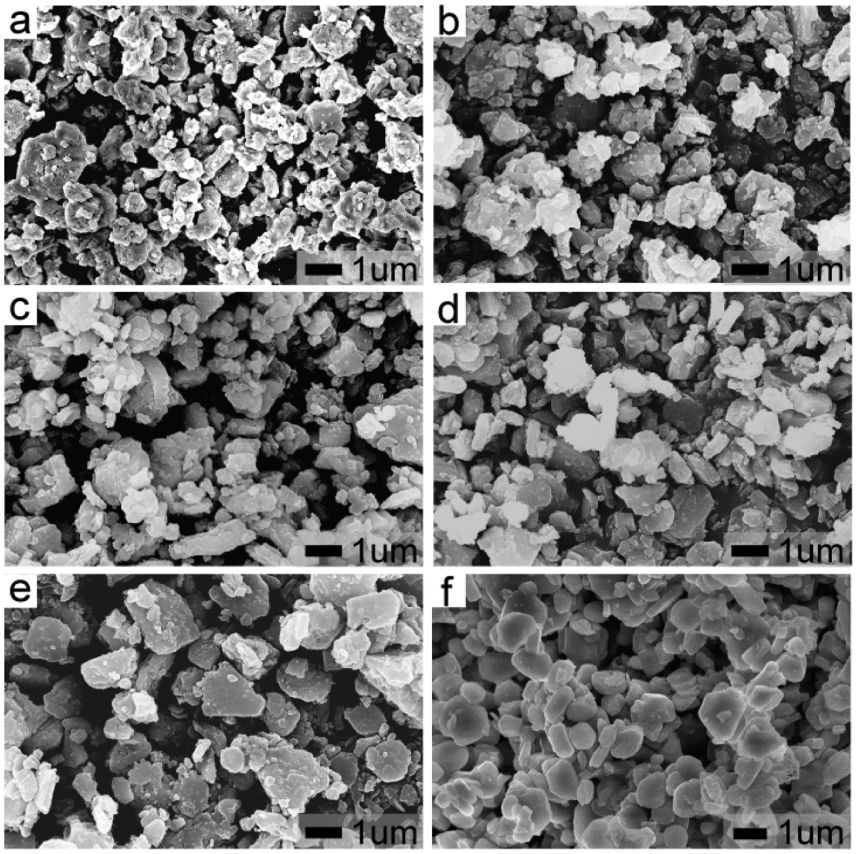

Figure 2. (a–f) SEM images of $NaFe_x(Ni_{0.5}Mn_{0.5})_{1-x}O_2$ samples with x = 0, 0.1, 0.2, 0.3, 0.4 and 1, respectively.

g^{-1} after 150 cycles,[26] while the Ti substitution in the O3-$NaFe_{0.2}(Ni_{1/2}Mn_{1/2})_{0.8}O_2$ even produced a higher capacity (145 mAh g^{-1}) and cycling stability over 200 cycles in a voltage range of 2.0–4.2 V.[27] These pioneering works suggest that the structural stability of O3-$NaFe_x(Ni_{1/2}Mn_{1/2})_{1-x}O_2$ phase can be considerably improved through an appropriate element substitution.

Nevertheless, the impacts of the Fe substitution on the sodium storage properties and structural change of the O3-$NaFe_x(Ni_{1/2}Mn_{1/2})_{1-x}O_2$ are not fully understood so far, especially at a wide work potential range (2–4.5 V). In this work, we have prepared a series of O3-$NaFe_x(Ni_{1/2}Mn_{1/2})_{1-x}O_2$ samples with x = 0, 0.1, 0.2, 0.3, 0.4, and 1 and investigated the structural evolutions of these materials during full charge process. The results reveal that the O3-Na-$Fe_x(Ni_{1/2}Mn_{1/2})_{1-x}O_2$ lattices with Fe substitution undergo different phase transformation at high charging potentials, and the Fe substitution can lead to a decreased interlayer distance, which can effectively suppress the co-insertion of the solvent components and therefore enhances the cycling stability of the material.

2. EXPERIMENTAL SECTION

2.1. Synthesis and Physicochemical Characterization. The nominal composition of $NaFe_x(Ni_{0.5}Mn_{0.5})_{1-x}O_2$ (x = 0, 0.1, 0.2, 0.3, 0.4) samples were prepared by a sol–gel method as described previously.[28] A mixed aqueous solution of sodium, iron, nickel, and manganese nitrates in a stoichiometric ratio was added to aqueous critic acid and then stirred for 6 h at 70 °C in water bath to form gel. The resulting gel was dried at 120 °C for 24 h and precalcined at 450 °C in air for 6 h to decompose the nitrate and organics. Finally, the

DOI: 10.1021/acsami.5b00594
ACS Appl. Mater. Interfaces 2015, 7, 8585–8591

powder precursor was ground and pressed into pellets and then calcined at 900 °C for 15 h in air atmosphere to obtain target materials. For the $NaNi_{0.5}Mn_{0.5}O_2$ sample, a recalcination process was conducted at 900 °C for 15 h to obtain pure-phase $NaNi_{0.5}Mn_{0.5}O_2$.

$NaFeO_2$ was prepared by solid-state method.[29] A stoichiometric amount of Fe_2O_3 and Na_2O_2 (with a 3% excess of sodium) was milled by high-energy mechanical milling (HEMM) and pressed into a pellet and then calcined at 650 °C for 12 h.

The lattice structures of the materials were characterized on an X-ray diffractometer (Shimadzu XRD-6000) using Cu Kα radiation scanning between 2θ = 10 and 80° at a rate of 2° min^{-1} and a step size of 0.02°. The electrode in ex situ X-ray diffraction (XRD) test was protected by a PE membrane, which can isolate the air and prevent H_2O in the air from intercalating into the material structure (the XRD peak of the PE membrane was omitted in the XRD pattern). The morphologies of the samples were observed by scanning electron microscope (FE-SEM, Zeiss Sigma).

2.2. Electrochemical Characterization. The electrodes used for electrochemical testing were fabricated by slurrying the active material, acetylene black, and PVdF binder in a weight ratio of 75:15:10 using *N*-methyl-pyrrolidone (NMP) as solvent and casting the slurry on aluminum foil collector. The 2016 type coin cells for charge−discharge measurements were assembled in a glovebox with water/oxygen content lower than 1 ppm. A Na disk was used as counter electrode and 1.0 mol L^{-1} $NaPF_6$ in ethylene carbonate/diethylcarbonate (EC/DEC, 50:50 vol %) solution was used as electrolyte. The galvanostatic charge/discharge tests were performed on a LAND cycler (Wuhan Kingnuo Electronic Co., China). Cyclic voltammetric measurements were carried out at a scan rate of 0.5 mV s^{-1} using a CHI 660a electrochemical workstation (ChenHua Instruments Co., China).

3. RESULTS AND DISCUSSION

3.1. Structural and Morphologic Features. Figure 1a shows the powder XRD patterns of $NaFe_x(Ni_{0.5}Mn_{0.5})_{1-x}O_2$ (x = 0, 0.1, 0.2, 0.3, 0.4, 1). The XRD patterns of the samples exhibit similar features and all of the diffraction peaks can be indexed to a hexagonal O3-structure with space group $R\bar{3}m$ (No. 167). The diffraction peaks of impurity are not observed for all the samples. The calculated hexagonal lattice parameters a and c are shown in Figure 1b, which increase linearly with the Fe content (x). It can be clarified by comparing the bond length of Fe−O (2.03 Å) in $NaFeO_2$[30] and 2.00 Å for (NiMn)−O bond in $NaNi_{0.5}Mn_{0.5}O_2$.[22,31] The increase of cell parameters with Fe amount agrees very well with the previous observations,[25] suggesting successful replacement of $Ni_{0.5}Mn_{0.5}$ with Fe to form $NaFe_x(Ni_{0.5}Mn_{0.5})_{1-x}O_2$ solid solution.

Figure 2 shows the morphologies of $NaFe_x(Ni_{0.5}Mn_{0.5})_{1-x}O_2$ (x = 0, 0.1, 0.2, 0.3, 0.4, 1) particles observed by scanning electron microscopy (SEM). The pristine $NaNi_{0.5}Mn_{0.5}O_2$ exhibits irregular particles with the size between 0.1 and 1.5 μm. By introducing Fe substitution, the layered $NaFe_x(Ni_{0.5}Mn_{0.5})_{1-x}O_2$ solid solution (x = 0.1, 0.2, 0.3, 0.4) displays slightly larger particle size. Further, a trend of particle growth is observed from x = 0.1 to x = 0.4. The morphology of $NaFeO_2$ prepared by solid state method is shown in Figure 2f, which exhibits small particle sizes with 0.5−0.8 μm due to the low synthetic temperature.

3.2. Electrochemical Performance. Figure 3 compares the cyclic voltammograms (CV) of the layered $NaFe_x(Ni_{0.5}Mn_{0.5})_{1-x}O_2$ (x = 0, 0.1, 0.2, 0.3, 0.4 and 1) samples at a scan rate of 0.5 mV s^{-1}. For the pristine $NaFe_x(Ni_{0.5}Mn_{0.5})_{1-x}O_2$ (x = 0) electrode, four pairs of reversible oxidation/reduction peaks appeared at 3.65/3.51, 3.49/3.41, 3.21/3.14, and 2.88/2.49 V, respectively, which represents multiple reversible phase transformations by Na/vacancy ordering in sodium layer or MO_2 slab in transition-metal layer.[7,25] Although the $NaFe_{0.1}Mn_{0.45}Ni_{0.45}O_2$ electrode exhibits the similar shape with the pristine $NaNi_{0.5}Mn_{0.5}O_2$, the CV peaks at >3.0 V became weaker and broader, implying a gentle transformation between the lattice phases. Furthermore, the redox couples observed at around 2.88/2.49 V in pristine sample shifts toward the higher potential region after Fe-substitution, which may related to the oxidation/reduction of Fe^{3+}/Fe^{4+} couple, which is evident by observed only one pair of redox peaks emerged at the potential region of 3.5−3 V for $NaFeO_2$ (Figure 3). When $x \geq 0.2$, substantial changes occur in the CV profiles, where only one broad oxidation band at 3.5 V and two broad reduction peaks at 2.75 and 3.45 V were observed, indicating that the multiphase transformation is restrained. This phenomenon could be accounted for by the suppression of MO_2 gliding and Na/vacancy ordering in the Na-intercalation process when Fe is introduced into the crystal lattice.[25] Furthermore, the CV curves of the Fe-substituted samples with different cycles overlap well compared with pristine $NaNi_{0.5}Mn_{0.5}O_2$, which demonstrates Fe substitution is beneficial to reaction reversibility. Therefore, it could be concluded that the Fe^{3+}/Fe^{4+} couple plays an important contribution to the reversible capacities of the Fe-substituted samples when charging to >3 V.

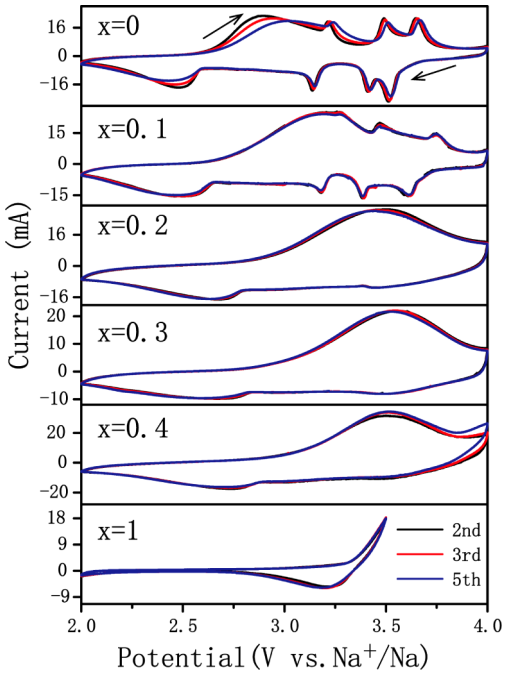

Figure 3. Cyclic voltammograms of $NaFe_x(Ni_{0.5}Mn_{0.5})_{1-x}O_2$ (x = 0, 0.1, 0.2, 0.3, 0.4 and 1) measured at a scan rate of 0.5 mV s^{-1}.

The suppression of the multiphase transformation can be also observed from the charge/discharge curves of the $NaFe_x(Ni_{0.5}Mn_{0.5})_{1-x}O_2$ electrodes. Figure 4 compares the galvanostatic charge/discharge profiles of the $NaFe_x(Ni_{0.5}Mn_{0.5})_{1-x}O_2$ (x = 0, 0.1, 0.2, 0.3, 0.4, and 1). The cells were tested with a current density of 0.05 C (12 mA g^{-1}) between 2.0 and 4.0 V. The charge/discharge curves of the pristine $NaNi_{0.5}Mn_{0.5}O_2$ obviously involve several voltage plateaus and steps, which reflect various Na/vacancy ordering and phase transformations occurring along with MO_2 slab gliding. At x = 0.1, the charge/discharge curves show slight changes compared to that of the pristine $NaNi_{0.5}Mn_{0.5}O_2$. The voltage plateaus become vague, which demonstrates that

DOI: 10.1021/acsami.5b00594
ACS Appl. Mater. Interfaces 2015, 7, 8585−8591

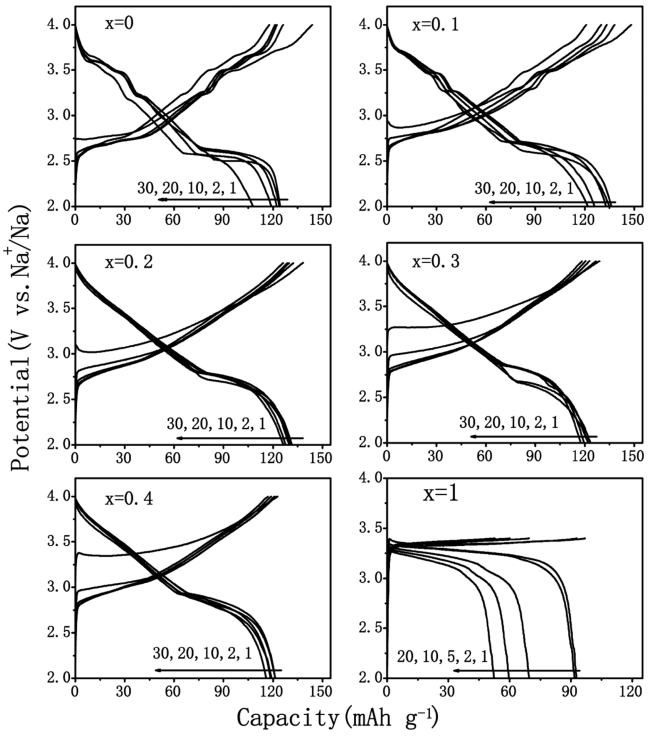

Figure 4. Charge−discharge curves of $NaFe_x(Ni_{0.5}Mn_{0.5})_{1-x}O_2$ (x = 0, 0.1, 0.2, 0.3, 0.4 and 1) cycled at a current rate of 12 mA g^{-1} (0.05 C).

introducing Fe element could suppress the phase conversion and is consistent with the CV curves. When $x \geq 0.2$ (x = 0.2, 0.3, 0.4), the charge/discharge profiles becomes smoother and can be divided into two main parts: a plateau around 2.7−2.9 V and a sloping part above 3.0 V. The voltage plateau is attributed to the phase transformation between O3 and P3 phases, while the sloping profile at higher voltage must be resulted from a solid-solution reaction with P3-structure. Obviously, introducing Fe element into the $NaNi_{0.5}Mn_{0.5}O_2$ lattice leads to a different Na-insertion mechanism due to the suppressed MO_2 gliding and phase conversion.[22] The reversible capacities obtained from the $NaFe_x(Ni_{0.5}Mn_{0.5})_{1-x}O_2$ samples are 124, 135, 131, 122, and 120 mAh g^{-1} for x = 0, 0.1, 0.2, 0.3, and 0.4, respectively, which exhibits a volcano shape dependence with the increase of Fe content. The pristine $NaNi_{0.5}Mn_{0.5}O_2$ in this work gave a reversible capacity of 124 mAh g^{-1}, which is similar to the value (125 mAh g^{-1}) obviously observed from FEC-free electrochemical solution.[22] When Fe content of x = 0.1 was introduced, the $NaFe_{0.1}(Ni_{0.5}Mn_{0.5})_{1-x}O_2$ cathode delivered an increased capacity of 135 mAh g^{-1}, which is most likely due to the decrease of the energy barrier for the two-phase conversion. However, as the Fe amount was further increased, the decrease in electrochemically active Ni content led to a decreased capacity of this material. Because pure $NaFeO_2$ can deliver only a reversible capacity of 92 mAh g^{-1}, much lower than $NaNi_{0.5}Mn_{0.5}O_2$, the Fe^{3+}/Fe^{4+} couple may have poorer electrochemical activity than that of the Ni^{2+}/Ni^{3+} couple in these composite oxide.

Figure 5a shows the cycling performance of the $NaFe_x(Ni_{0.5}Mn_{0.5})_{1-x}O_2$ electrodes. The capacity of pristine $NaNi_{0.5}Mn_{0.5}O_2$ decreases from 124 to 108 mAh g^{-1} during 30 cycles, corresponding to a capacity retention of 87%. In comparison, the $NaFe_x(Ni_{0.5}Mn_{0.5})_{1-x}O_2$ sample with x = 0.1 shows a slightly higher capacity retention of 89%, reflecting an increased structural stability of the substituted sample. With increasing the Fe amount, the $NaFe_x(Ni_{0.5}Mn_{0.5})_{1-x}O_2$ cathodes demonstrate remarkable improvement in their cycle stability, giving a capacity retention of 96.4, 95.2, and 95.4% when x = 0.2, 0.3, and 0.4, respectively. In contrast, the $NaFeO_2$ electrode exhibits very fast capacity degradation from 92 mAh g^{-1} in the first cycle to 42 mAh g^{-1} after 28 cycles, corresponding to only 46% capacity retention. This poor cyclability is known to result from the Fe^{4+} migration from the transition-metal layer to sodium layer, arising from FeO_6 octahedral distortion of Jahn−Teller effect.[29] This mechanism can also account for the decreased cyclability of the highly Fe-substituted samples. Yabuuchi et al. reported that the x = 0.6 sample had worse cycling performance than the x = 0.4 sample.[25] Additionally, the high Fe-substituted samples also show lower reversible capacity due to the poorer electrochemical activity of the Fe^{3+}/Fe^{4+} couple as discussed above and in previous work.[25] Therefore, as a good compromise of the reversible capacity and cycling stability, the $NaFe_{0.2}Mn_{0.4}Ni_{0.4}O_2$ in this work is an optimum choice for high-performance sodium storage cathode material.

The effect of Fe substitution on the rate capability of the $NaFe_x(Ni_{0.5}Mn_{0.5})_{1-x}O_2$ was also investigated for its possible high-power applications. Figure 5b shows the discharge capacities of pristine $NaNi_{0.5}Mn_{0.5}O_2$ and $NaFe_{0.2}Mn_{0.4}Ni_{0.4}O_2$ at changing discharge rates. The $NaFe_{0.2}Mn_{0.4}Ni_{0.4}O_2$ electrode

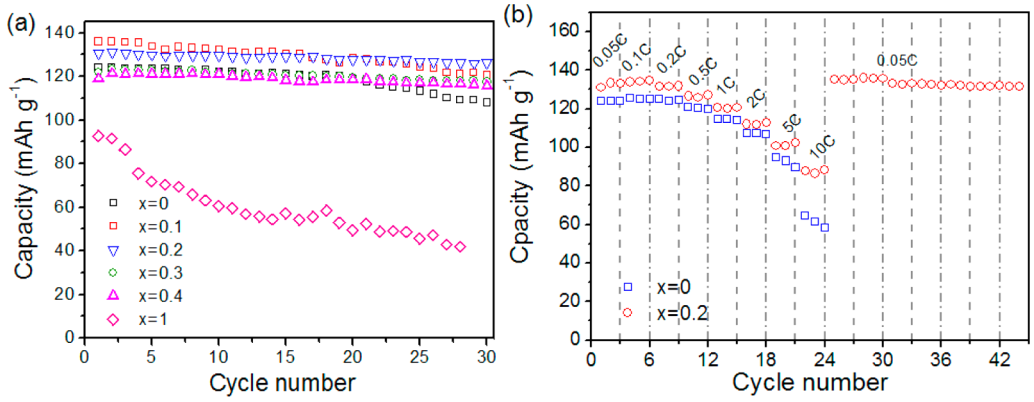

Figure 5. (a) Cycling capacities of the $NaFe_x(Ni_{0.5}Mn_{0.5})_{1-x}O_2$ (x = 0, 0.1, 0.2, 0.3, 0.4, 1) cycled at a current rate of 12 mA g^{-1} (0.05 C). (b) Rate capability of the $NaMn_{0.4}Ni_{0.4}O_2$ and $NaFe_{0.2}Mn_{0.4}Ni_{0.4}O_2$ samples. Samples were charged at a rate of 12 mA g^{-1} (0.05 C) and then discharged at different rates, 12 mA g^{-1} (0.05 C) ~ 2400 mA g^{-1} (10 C).

DOI: 10.1021/acsami.5b00594
ACS Appl. Mater. Interfaces 2015, 7, 8585−8591

can deliver a much higher reversible capacity of 133, 133, 131, 125, 120, 112, 100, and 86 mAh g^{-1} at current rates of 12 (0.05 C), 24 (0.1 C), 48 (0.2 C), 120 (0.5 C), 240 (1 C), 480 (2 C), and 1200 (5 C), respectively. Even at a very high rate of 2400 mA g^{-1} (10 C), the $NaFe_{0.2}Mn_{0.4}Ni_{0.4}O_2$ electrode can still deliver 64% of its capacity, whereas the $NaNi_{0.5}Mn_{0.5}O_2$ electrode can only deliver a capacity of 61 mAh g^{-1} at 10 C. The excellent rate capability of the $NaFe_{0.2}Mn_{0.4}Ni_{0.4}O_2$ electrode could be attributed to the suppressed phase transformations and larger interslab distance after Fe substitution, which leads to fast ionic diffusion between the interslabs. Besides, when the charge/discharge rate was adjusted back to 0.05 C, this electrode can recover its full capacity and keep at 130 mAh g^{-1} during subsequent cycles.

To further enhance the reversible capacity, the charge voltage was extended to a higher region. Figure 6 displays CV curves of

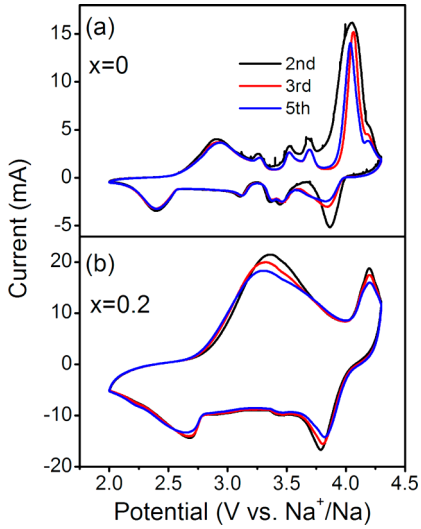

Figure 6. CV of (a) $NaNi_{0.5}Mn_{0.5}O_2$ and (b) $NaFe_{0.2}Ni_{0.4}Mn_{0.4}O_2$ cycled between 4.3 and 2 V.

the $NaFe_x(Ni_{0.5}Mn_{0.5})_{1-x}O_2$ (x = 0, 0.2) at a wider voltage range of 2.0–4.3 V with a scan rate of 0.5 mV s^{-1}. The CV curves of both the electrodes show a pair of new anodic/cathodic peaks at high voltages of ~4.1/3.86 V, representing the oxidation/reduction reactions of Ni^{3+}/Ni^{4+} couple along with Na^+ removal/insertion. However, these two electrodes show different CV feature at the high potential region: the oxidation peak of $NaNi_{0.5}Mn_{0.5}O_2$ electrode at 4.1 V is much stronger than its reduction peak at 3.86 V, and the peak intensity fades quickly with subsequent cycles, indicating an irreversible electrochemical reaction. This irreversible reaction has been speculated to the co-insertion of the electrolyte solvent at high charge voltage due to the larger interslab distance of $NaNi_{0.5}Mn_{0.5}O_2$.[22] In comparison, the $NaFe_{0.2}Mn_{0.4}Ni_{0.4}O_2$ electrode shows more symmetrical redox peaks at 3.8/4.2 V and well-overlapped cycle profiles, indicating that the Fe-substituted sample have higher reversibility of Na-ion insertion and extraction at high voltage charge. This difference can also be observed clearly from the charge/discharge profiles of these two electrodes. Figure 7 displays the galvanstatic charge/discharge profiles of $NaFe_x(Ni_{0.5}Mn_{0.5})_{1-x}O_2$ (x = 0, 0.2) at a current rate of 0.05 C. Both electrodes exhibit high charge/discharge plateaus at 4.15/4.0 V, but the $NaNi_{0.5}Mn_{0.5}O_2$ electrode gives a much larger

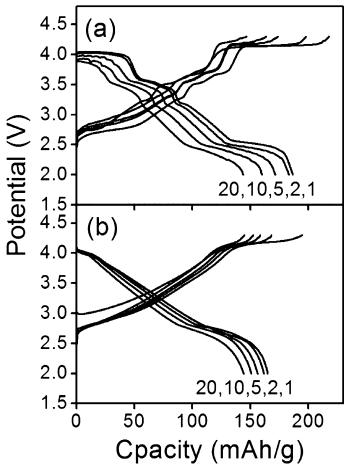

Figure 7. Charge–discharge curves of (a) $NaNi_{0.5}Mn_{0.5}O_2$ and (b) $NaFe_{0.2}Ni_{0.4}Mn_{0.4}O_2$ cycled between 4.3 and 2 V.

charge capacity and a similar discharge capacity to the $NaFe_{0.2}Mn_{0.4}Ni_{0.4}O_2$ electrode, suggesting lower coulombic efficiency than its Fe-substituted counterpart. After the extended charge, the $NaNi_{0.5}Mn_{0.5}O_2$ delivered an initial reversible capacity of 186 mAh g^{-1}, higher than its discharge capacity (124 mAh g^{-1}) cycled in 4.0–2.0 V. However, the cycling capacities decrease gradually down to 144 mAh g^{-1} after 20 cycles, corresponding to 78% capacity retention. This capacity decay occurs mainly at high voltage region, indicating an unstable phase transformation at high voltage charge. For comparison, the $NaFe_{0.2}Mn_{0.4}Ni_{0.4}O_2$ exhibits better capacity retention (87%) over 20 cycles, though its initial capacity (165 mAh g^{-1}) is slightly lower. This further confirms that the Fe substitution can improve the structural stability of the material.

3.3. Structure Evolution in Na^+ Extraction Process. To further investigate the effect of Fe-substitution on the structural evolution in the full Na insertion process, the ex situ XRD patterns of the $NaFe_x(Ni_{0.5}Mn_{0.5})_{1-x}O_2$ (x = 0, 0.2) samples were recorded at different charge states. Figure 8a shows the ex situ XRD patterns of the $NaNi_{0.5}Mn_{0.5}O_2$ charged to 4 and 4.3 V. When the electrode charged to 4.0 V, its $(006)_{O3}$ and $(104)_{O3}$ peaks at 33 and 42° disappear and a new peak at 31° appears, characterizing a phase transformation from O3 to P3. When further charged to 4.3 V, the XRD pattern exhibits a similar phase structure to that obtained at 4.0 V, but the relative intensities of the peaks change considerably, suggesting a further phase transformation from P3 to P3″.[22] It is worth noting that peaks around 12 and 25° do not appear in the XRD pattern at 4.3 V, which is different from that previously reported.[22] Actually, we used the protective membrane to prevent the moisture from moving into the material structure during the ex situ XRD test. To further elucidate the difference in the XRD pattern, we uncovered the protective membrane to expose the electrode charged at 4.3 V to air for 5 min and tested XRD pattern again. In the XRD pattern for the sample exposed to air appears new peaks around 12° and 25° (Figure 8a). This result demonstrates that the peaks appeared at 12.7 and 25.3° should be attributed to the intercalation into the MO_2 layers of water molecules that come from the air.[32,33] Furthermore, the (003) peak gradually shifts toward a lower angle from the initial potential to 4.3 V, indicating that the d-distance of (003) peak increases during charge from 5.33 Å at the starting potential (O3) to 5.72 Å at 4.3 V (P3″). Such a

DOI: 10.1021/acsami.5b00594
ACS Appl. Mater. Interfaces 2015, 7, 8585–8591

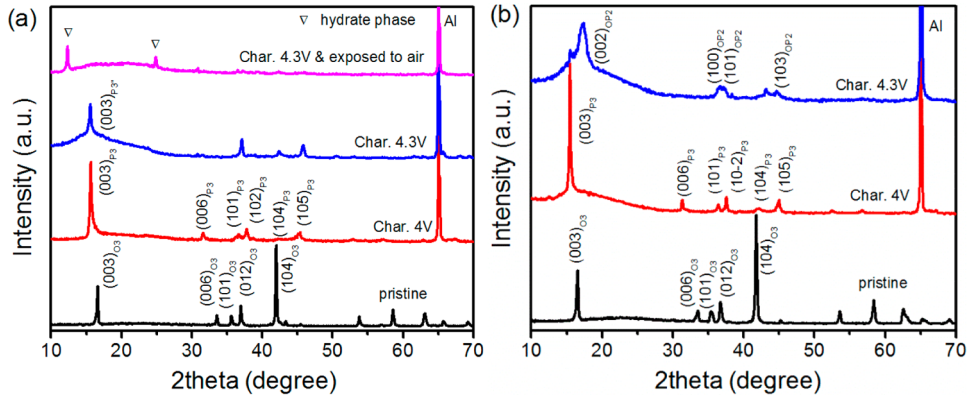

Figure 8. Ex situ XRD patterns of the of $NaFe_x(Ni_{0.5}Mn_{0.5})_{1-x}O_2$ electrodes at various charge state, (a) $x = 0$, (b) $x = 0.2$.

large interslab distance of the P3″ phase have been speculated to allow the electrolyte molecule or large anions to insert into the MO_2 layers,[22] thus leading to a low coulombic efficiency and poor cycling stability (Figure. 7a). For the Fe-substituted sample ($NaFe_{0.2}Ni_{0.4}Mn_{0.4}O_2$), the reversibility of the two-phase transformation between O3 and P3 was also found when the sample was charged to 4 V. As shown in Figure 8b, the Fe substitution does not change the two-phase transition mechanism but only suppresses the Na/vacancy ordering, so that the $NaFe_{0.2}Ni_{0.4}Mn_{0.4}O_2$ electrode exhibits better structural stability (Figure. 5a).

Nevertheless, it could also be observed that one new XRD peak at 17° appeared at the charge potential of 4.3 V, which differs from the P3″ phase of the unsubstituted sample (Figure 8a), indicating an appearance of a new phase. Based on the previous report,[23] this new phase could be assigned to a OP2 phase, which is analogous to the phase transformation of the O3-type $NaFe_{0.5}Mn_{0.5}O_2$.[23] Compared to the $NaNi_{0.5}Mn_{0.5}O_2$, the different phase transformation of the $NaFe_{0.2}Ni_{0.4}Mn_{0.4}O_2$ obviously results from the substitution of Fe. The $(002)_{OP2}$ peak of OP2 phase shifts to a higher angle, corresponding to the reduction of the slab distance. Komaba's group has reported that iron migration in $NaFeO_2$ can occur from the MO_2 layer to Na layer when charged to higher voltage.[29] Therefore, it might be speculated that when charged to 4.3 V, some Fe ions can migrate from octahedron in transition-metal layers to interstitial tetragon sites or octahedron sites in sodium layers to increase the electrostatic attraction of two oxygen layers, thus leading to a decrease of the interslab distance. Calculated from the data of Figure 8b, the interslab distance of the $NaFe_{0.2}Ni_{0.4}Mn_{0.4}O_2$ increases first from 5.36 to 5.69 Å at 4.0 V and then decreases to 5.13 Å at 4.3 V. Apparently, the decrease of the interslab distance can alleviate effectively the insertion of the electrolyte molecule or large anions between two MO_2 layers, resulting in an improved structural stability (Figure 7) if compared to the larger interslab distance (5.72 Å) of P3″–$Na_xNi_{0.5}Mn_{0.5}O_2$.

4. CONCLUSIONS

In summary, we prepared a series of O3-phase $NaFe_x(Ni_{0.5}Mn_{0.5})_{1-x}O_2$ ($x = 0$, 0.1, 0.2, 0.3, 0.4) samples by simple sol–gel method. The electrochemical characterization reveals that the substitution of Fe has an important influence on electrochemical performance of $NaFe_x(Ni_{0.5}Mn_{0.5})_{1-x}O_2$ in terms of the reversible capacity, cycling capability, and rate performance, due to a strong suppression of the Na/vacancy ordering. The $NaFe_{0.2}Mn_{0.4}Ni_{0.4}O_2$ with an optimized Fe content ($x = 0.2$) can delivers an initial capacity of 131 mAh g^{-1} and >95% capacity retention ratio over 30 cycles. In addition, this electrode also exhibits a high rate capability with 64% capacity retention at 10 C, considerably higher than the unsubstituted samples. Ex situ XRD characterizations show similar structural evolution from O3 to P3 between 2.0 and 4.0 V for both the $NaFe_{0.2}Mn_{0.4}Ni_{0.4}O_2$ and $NaNi_{0.5}Mn_{0.5}O_2$ electrodes. However, different structure transformations were found for $NaNi_{0.5}Mn_{0.5}O_2$ and $NaFe_{0.2}Mn_{0.4}Ni_{0.4}O_2$, which underwent P3–P3″ and P3–OP2 transformations respectively in a voltage range of 4.0–4.3 V. This difference originates from the Fe substitution, which causes the migration of Fe ions from octahedron in transiton-metal layer to interstitial tetrahedron or octahedron sites in sodium layers, thus decreasing the interslab distance by increasing the electrostatic attraction between two oxygen layers. Therefore, the Fe substitution could provide smooth phase transformation to improve the reversible capacity and cycling stability, thus making the Fe-substitution oxide possible as a promising cathode material for high-performance sodium ion batteries. Most significantly, the Fe substitution also contributes a stable phase transformation (OP2 phase) in the high voltage range (>4.0 V) to enhance the structural stability. This new finding may offer a new strategy for design of high capacity and high stability cathode materials for sodium-ion batteries.

AUTHOR INFORMATION

Corresponding Author

*E-mail: ylcao@whu.edu.cn. Tel.: +86-027-68754526.

Author Contributions

All authors contributed equally to this work. Y.C. conceived the idea of the serial Na-host material; D.Y. and Y.W. directed the experimental work and conducted the measurements. Y.C. and H.Y. wrote the paper. All authors participated in analyzing the experimental data and discussing the results, as well as preparing the paper.

Notes

The authors declare no competing financial interest.

ACKNOWLEDGMENTS

We are thankful for financial support from the National Basic Research Program of China (No. 2015CB251100), the National Science Foundation of China (Nos. 2133307 and 21373155), and the Program for New Century Excellent Talents in University (NCET-12-0419).

DOI: 10.1021/acsami.5b00594
ACS Appl. Mater. Interfaces 2015, 7, 8585–8591

REFERENCES

(1) Slater, M. D.; Kim, D.; Lee, E.; Johnson, C. S. Sodium-Ion Batteries. *Adv. Funct. Mater.* **2013**, *23* (8), 947−958.

(2) Pan, H.; Hu, Y.-S.; Chen, L. Room-Temperature Stationary Sodium-Ion Batteries for Large-Scale Electric Energy Storage. *Energy Environ. Sci.* **2013**, *6* (8), 2338.

(3) Armand, M.; Tarascon, J. M. Building Better Batteries. *Nature* **2008**, *451* (7179), 652−657.

(4) Cao, Y.; Xiao, L.; Sushko, M. L.; Wang, W.; Schwenzer, B.; Xiao, J.; Nie, Z.; Saraf, L. V.; Yang, Z.; Liu, J. Sodium Ion Insertion in Hollow Carbon Nanowires for Battery Applications. *Nano Lett.* **2012**, *12* (7), 3783−3787.

(5) Ding, J.; Wang, H.; Li, Z.; Kohandehghan, A.; Cui, K.; Xu, Z.; Zahiri, B.; Tan, X.; Lotfabad, E. M.; Olsen, B. C.; Mitlin, D. Carbon Nanosheet Frameworks Derived from Peat Moss As High Performance Sodium Ion Battery Anodes. *ACS Nano* **2013**, *7* (12), 11004−15.

(6) Wu, L.; Hu, X.; Qian, J.; Pei, F.; Wu, F.; Mao, R.; Ai, X.; Yang, H.; Cao, Y. Sb−C Nanofibers with Long Cycle Life As an Anode Material for High-Performance Sodium-Ion Batteries. *Energy Environ. Sci.* **2014**, *7* (1), 323.

(7) Berthelot, R.; Carlier, D.; Delmas, C. Electrochemical Investigation of the P2−Na_xCoO_2 Phase Diagram. *Nat. Mater.* **2011**, *10* (1), 74−80.

(8) Guignard, M.; Didier, C.; Darriet, J.; Bordet, P.; Elkaïm, E.; Delmas, C. P2-Na_xVO_2 System As Electrodes for Batteries and Electron-Correlated Materials. *Nat. Mater.* **2013**, *12* (1), 74−80.

(9) Ma, X.; Chen, H.; Ceder, G. Electrochemical Properties of Monoclinic $NaMnO_2$. *J. Electrochem. Soc.* **2011**, *158* (12), A1307−A1312.

(10) Yuan, D.; Liang, X.; Wu, L.; Cao, Y.; Ai, X.; Feng, J.; Yang, H. A Honeycomb-Layered $Na_3Ni_2SbO_6$: A High-Rate and Cycle-Stable Cathode for Sodium-Ion Batteries. *Adv. Mater.* **2014**, *26* (36), 6301−6.

(11) Hasa, I.; Buchholz, D.; Passerini, S.; Hassoun, J. A Comparative Study of Layered Transition Metal Oxide Cathodes for Application in Sodium-Ion Battery. *Acs Appl. Mater. Interfaces* **2015**, *7* (9), 5206−5212.

(12) Lim, S. Y.; Kim, H.; Chung, J.; Lee, J. H.; Kim, B. G.; Choi, J. J.; Chung, K. Y.; Cho, W.; Kim, S. J.; Goddard, W. A., 3rd; Jung, Y.; Choi, J. W. Role of Intermediate Phase for Stable Cycling of $Na_7V_4(P_2O_7)_4PO_4$ in Sodium Ion Battery. *Proc. Natl. Acad. Sci. U.S.A.* **2014**, *111* (2), 599−604.

(13) Serras, P.; Palomares, V.; Alonso, J.; Sharma, N.; López del Amo, J. M.; Kubiak, P.; Fdez-Gubieda, M. L.; Rojo, T. Electrochemical Na Extraction/Insertion of $Na_3V_2O_{2x}(PO_4)_2F_{3-2x}$. *Chem. Mater.* **2013**, *25* (24), 4917−4925.

(14) Saravanan, K.; Mason, C. W.; Rudola, A.; Wong, K. H.; Balaya, P. The First Report on Excellent Cycling Stability and Superior Rate Capability of $Na_3V_2(PO_4)_3$ for Sodium Ion Batteries. *Adv. Energy Mater.* **2013**, *3* (4), 444−450.

(15) Li, H.; Bai, Y.; Wu, F.; Li, Y.; Wu, C. Budding Willow Branches Shaped $Na_3V_2(PO_4)_3$/C Nanofibers Synthesized via an Electrospinning Technique and Used As Cathode Material for Sodium Ion Batteries. *J. Power Sources* **2015**, *273* (0), 784−792.

(16) Qian, J.; Zhou, M.; Cao, Y.; Ai, X.; Yang, H. Nanosized $Na_4Fe(CN)_6$/C Composite as a Low-Cost and High-Rate Cathode Material for Sodium-Ion Batteries. *Adv. Energy Mater.* **2012**, *2* (4), 410−414.

(17) Wu, X.; Deng, W.; Qian, J.; Cao, Y.; Ai, X.; Yang, H. Single-Crystal $FeFe(CN)_6$ Nanoparticles: A High Capacity and High Rate Cathode for Na-Ion Batteries. *J. Mater. Chem. A* **2013**, *1* (35), 10130−10134.

(18) Wang, L.; Lu, Y.; Liu, J.; Xu, M.; Cheng, J.; Zhang, D.; Goodenough, J. B. a Superior Low-Cost Cathode for a Na-Ion Battery. *Angew. Chem., Int. Ed. Engl.* **2013**, *52* (7), 1964−7.

(19) Delmas, C.; Fouassier, C.; Hagenmuller, P. Structural Classification and Properties of the Layered Oxides. *Physica B+C* **1980**, *99* (1−4), 81−85.

(20) Lei, Y. C.; Li, X.; Liu, L.; Ceder, G. Synthesis and Stoichiometry of Different Layered Sodium Cobalt Oxides. *Chem. Mater.* **2014**, *26* (18), 5288−5296.

(21) Lu, Z.; Dahn, J. R. In Situ X-Ray Diffraction Study of P2-$Na_{2/3}[Ni_{1/3}Mn_{2/3}]O_2$. *J. Electrochem. Soc.* **2001**, *148* (11), A1225−A1229.

(22) Komaba, S.; Yabuuchi, N.; Nakayama, T.; Ogata, A.; Ishikawa, T.; Nakai, I. Study on the Reversible Electrode Reaction of $Na_{1-x}Ni_{0.5}Mn_{0.5}O_2$ for a Rechargeable Sodium-Ion Battery. *Inorg. Chem.* **2012**, *51* (11), 6211−20.

(23) Yabuuchi, N.; Kajiyama, M.; Iwatate, J.; Nishikawa, H.; Hitomi, S.; Okuyama, R.; Usui, R.; Yamada, Y.; Komaba, S. P2-type $Na_x[Fe_{1/2}Mn_{1/2}]O_2$ Made from Earth-Abundant Elements for Rechargeable Na Batteries. *Nat. Mater.* **2012**, *11* (6), 512−517.

(24) Komaba, S.; Nakayama, T.; Ogata, A.; Shimizu, T.; Takei, C.; Takada, S.; Hokura, A.; Nakai, I. Electrochemically Reversible Sodium Intercalation of Layered $NaNi_{0.5}Mn_{0.5}O_2$ and $NaCrO_2$. *ECS Trans.* **2009**, *16* (42), 43−55.

(25) Yabuuchi, N.; Yano, M.; Yoshida, H.; Kuze, S.; Komaba, S. Synthesis and Electrode Performance of O3-Type $NaFeO_2$-$NaNi_{1/2}Mn_{1/2}O_2$ Solid Solution for Rechargeable Sodium Batteries. *J. Electrochem. Soc.* **2013**, *160* (5), A3131−A3137.

(26) Kim, D.; Lee, E.; Slater, M.; Lu, W.; Rood, S.; Johnson, C. S. Layered $Na[Ni_{1/3}Fe_{1/3}Mn_{1/3}]O_2$ cathodes for Na-Ion battery application. *Electrochem. Commun.* **2012**, *18*, 66−69.

(27) Sun, X.; Jin, Y.; Zhang, C.-Y.; Wen, J.-W.; Shao, Y.; Zang, Y.; Chen, C.-H. $Na[Ni_{0.4}Fe_{0.2}Mn_{0.4-x}Ti_x]O_2$: A Cathode of High Capacity and Superior Cyclability for Na-Ion Batteries. *J. Mater. Chem. A* **2014**, *2* (41), 17268−17271.

(28) Yuan, D.; He, W.; Pei, F.; Wu, F.; Wu, Y.; Qian, J.; Cao, Y.; Ai, X.; Yang, H. Synthesis and Electrochemical Behaviors of Layered $Na_{0.67}[Mn_{0.65}Co_{0.2}Ni_{0.15}]O_2$ Microflakes As a Stable Cathode Material for Sodium-Ion Batteries. *J. Mater. Chem. A* **2013**, *1* (12), 3895.

(29) Yabuuchi, N.; Yoshida, H.; Komaba, S. Crystal Structures and Electrode Performance of Alpha-$NaFeO_2$ for Rechargeable Sodium Batteries. *Electrochemistry* **2012**, *80* (10), 716−719.

(30) Takeda, Y.; Nakahara, K.; Nishijima, M.; Imanishi, N.; Yamamoto, O.; Takano, M.; Kanno, R. Sodium Deintercalation from Sodium Iron Oxide. *Mater. Res. Bull.* **1994**, *29* (6), 659−666.

(31) Oh, S.-M.; Myung, S.-T.; Jang, M.-W.; Scrosati, B.; Hassoun, J.; Sun, Y.-K. An Advanced Sodium-Ion Rechargeable Battery Based on a Tin-Carbon Anode and a Layered Oxide Framework Cathode. *Phys. Chem. Chem. Phys.* **2013**, *15* (11), 3827−3833.

(32) Lu, Z.; Dahn, J. R. Intercalation of Water in P2, T2 and O2 Structure $A_z[Co_xNi_{1/3-x}Mn_{2/3}]O_2$. *Chem. Mater.* **2001**, *13* (4), 1252−1257.

(33) Wang, X.; Liu, G.; Iwao, T.; Okubo, M.; Yamada, A. Role of Ligand-to-Metal Charge Transfer in O3-Type $NaFeO_2$−$NaNiO_2$ Solid Solution for Enhanced Electrochemical Properties. *J. Phys. Chem. C* **2014**, *118* (6), 2970−2976.

DOI: 10.1021/acsami.5b00594
ACS Appl. Mater. Interfaces 2015, 7, 8585−8591